

# A Mixer Layer is Worth One Graph Convolution: Unifying MLP-Mixers and GCNs for Human Motion Prediction

Xinshun Wang  
Sun Yat-sen University

Shen Zhao  
Sun Yat-sen University

Chen Chen  
University of Central Florida

Mengyuan Liu  
Peking University

## Abstract

The past few years has witnessed the dominance of Graph Convolutional Networks (GCNs) over human motion prediction, while their performance is still far from satisfactory. Recently, MLP-Mixers show competitive results on top of being more efficient and simple. To extract features, GCNs typically follow an aggregate-and-update paradigm, while Mixers rely on token mixing and channel mixing operations. The two research paths have been independently established in the community. In this paper, we develop a novel perspective by unifying Mixers and GCNs. We show that a mixer layer can be seen as a graph convolutional layer applied to a fully-connected graph with parameterized adjacency. Extending this theoretical finding to the practical side, we propose Meta-Mixing Network ( $M^2$ -Net). Assisted with a novel zero aggregation operation, our network is capable of capturing both the structure-agnostic and the structure-sensitive dependencies in a collaborative manner. Not only is it computationally efficient, but most importantly, it also achieves state-of-the-art performance. An extensive evaluation on the Human3.6M, AMASS, and 3DPW datasets shows that  $M^2$ -Net consistently outperforms all other approaches. We hope our work brings the community one step further towards truly predictable human motion. Our code will be publicly available.

## 1. Introduction

The idea of predictable human motion has attracted much research interest over the years across a wide range of applications such as human-robot interaction and autonomous driving. Since their inception, Graph Convolutional Networks (GCNs) [17] have occupied a dominant place in human motion prediction [28, 29, 25, 22, 30, 4, 32], partially due to the observation that human body is naturally a graph with joints being nodes and bones being edges. Re-

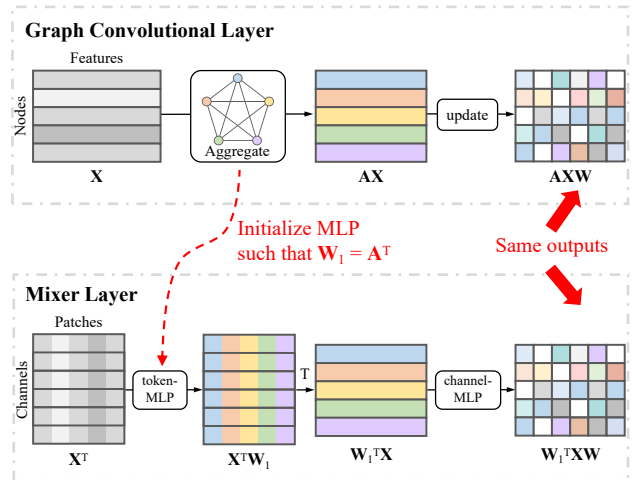


Figure 1. **Comparison between MLP-Mixers and GCNs.** GCNs typically follow an aggregate-and-update paradigm, while MLP-Mixers employ token mixing and channel mixing. Though developed from distinct theoretical motivations, MLP-Mixers and GCNs bear a strong analogy in terms of how the individual layer looks. A Mixer layer can be seen as a graph convolutional layer applied to a fully-connected graph with parameterized adjacency.

cently, GCN-based methods appear to have plateaued, as the community witnesses more novel GCN variations with millions of parameters and only millimeter-level improvement, while a predictable future still seems far out of reach of what GCNs can achieve. Meanwhile in computer vision, led by MLP-Mixer [33], there emerges a prominent line of research [14, 34, 38, 5, 24] which investigates the benefits of using multi-layer perceptrons (MLPs). Simply put, they pitch the idea of pure MLP-based networks, the selling point being their competitive performance along with elegant simplicity and efficiency. The idea of MLP-Mixer has been leveraged into human motion prediction recently. Several Mixer-like methods [13, 1] show state-of-the-art

performance on top of being considerably simple and efficient, providing a lesson in what we can achieve by doing away with graphs entirely. GCNs and Mixer models have each been established independently in the community. Their competitive performance to one another begs the question: What is the difference and connection between the theoretical underpinnings of Mixers and GCNs?

We answer this by providing a unified perspective on Mixers and GCNs. Given an  $N \times D$  matrix  $\mathbf{X} = [\mathbf{x}_1, \mathbf{x}_2, \dots, \mathbf{x}_N]^\top$  of  $N$  patches with  $D$  features as input, each mixer layer applies channel-mixing and token-mixing in successive order. From a matrix operation point of view, their overall effect is a combination of matrix products  $\mathbf{W}_1^\top \mathbf{X} \mathbf{W}_2$ , where  $\mathbf{W}_1$  is an  $N \times N$  weight matrix and  $\mathbf{W}_2$  is a  $D \times D$  weight matrix, which are implicitly given by the channel-mixing MLP and token-mixing MLP respectively. The mixer layer bears a strong analogy to the graph convolutional layer in standard GCNs, which follows an aggregate-update paradigm. The aggregation and update also result in a combination of matrix products  $\mathbf{A} \mathbf{X} \mathbf{W}$ , where  $\mathbf{A}$  is an  $N \times N$  adjacency matrix for aggregation and  $\mathbf{W}$  is a  $D \times D$  weight matrix for update. Comparing the mixer layer and the graph convolutional layer, we make the following two findings. First, the update is the same as token-mixing. Second, the aggregation and channel-mixing both perform a linear combination of node or patch features (rows in  $\mathbf{X}$ ). The main takeaway is that a mixing layer can be seen as a graph convolutional layer applied to a fully-connected graph with parameterized adjacency, which raises the second question: How can this unified perspective benefit the community on the practical side?

We address this question by proposing Meta-Mixing Network (M<sup>2</sup>-Net), which is developed from the unified perspective discussed above. Our network unifies Mixers and GCNs, exploiting their collaborative advantages in extracting structure-specific and structure-agnostic features, which is crucial for the task because human motion is intrinsically controlled by one’s skeleton, while diverse motion patterns share similarity regardless of the individual skeleton. Its building block, Meta-Mixer, employs a novel “zero aggregation”, where manually specified elements of the parameterized adjacency grow from zeros to optimized parameters in a learned manner. By using the proposed zero aggregation along with parameter tying, the network is able to capture both the structure-sensitive and structure-independent dependencies in a collaborative manner in spatial-temporal domain. Therefore, our network is more than a simple combination of two models, but rather a unique one that unifies two approaches to unleash their collaborative power.

In summary, our contributions are three-fold:

- We develop a unified perspective on GCNs and Mixers, showing that a mixer layer can be seen as a graph convolutional layer applied to a fully-connected graph

with parameterized adjacency. Based on this finding, we unify them into a novel Meta-Mixer, which exploits their collaborative advantages in modeling structure-sensitive and structure-independent information.

- We propose Meta-Mixing Network based on the Meta-Mixer. Its building blocks include spatial Meta-Mixers and temporal Meta-Mixers. With a novel zero aggregation operation that we propose, they are able to capture both the structure-specific and structure-agnostic dependencies in a refining manner.
- We conduct extensive experiments which highlight the benefits of unifying Mixers and GCNs into the proposed Meta-Mixer. Our Meta-Mixing Network outperforms state-of-the-art approaches by large margins on Human3.6M, AMASS and 3DPW datasets.

## 2. Related Work

**GCN-based human motion prediction.** In recent years human motion prediction has been dominated almost exclusively by GCNs. [28] is among the first to leverage GCNs into human motion prediction, proposing to represent the human skeleton as a learnable fully-connected graph. It shows the exceptional capability of GCNs compared to RNNs and CNNs [9, 10, 11, 3, 19] at the time, blazing a trail followed by many works which focus on improving the design of GCNs to specifically exploit the human body structure and motion patterns. A subsequent work [7] introduces a graph with predefined topology based on human skeletal structure. Besides the original skeleton level, human motion can be modeled at different levels using multi-scale graphs [22, 8, 23, 40]. Regarding the defining step in GCNs which is graph convolution [17], the graph convolution initially used in early approaches [28, 8] involves simple matrix multiplication and a trainable adjacency matrix. Later approaches [7] additionally employ temporal CNNs [18] to learn temporal dependencies. [23, 25] implement the graph convolution layer using two adjacency matrices defined in spatial and temporal domains respectively. Motivated by depth-wise separable convolution [6] applied in CNNs, [30] proposes a novel space-time-separable graph convolution. [20, 21] has investigated the benefits of using spectral GCNs [2], which combine graph spectral analysis with graph networks.

**Mixer-like models.** Our work is also related to MLP-Mixer [33] and a few Mixer-like models that undertake similar designs. In a general sense, the research in computer vision has come full circle back to MLPs, showcased by a prominent line of works [33, 34, 14, 38, 12, 31, 35] showing that pure MLP-based networks, when combined with

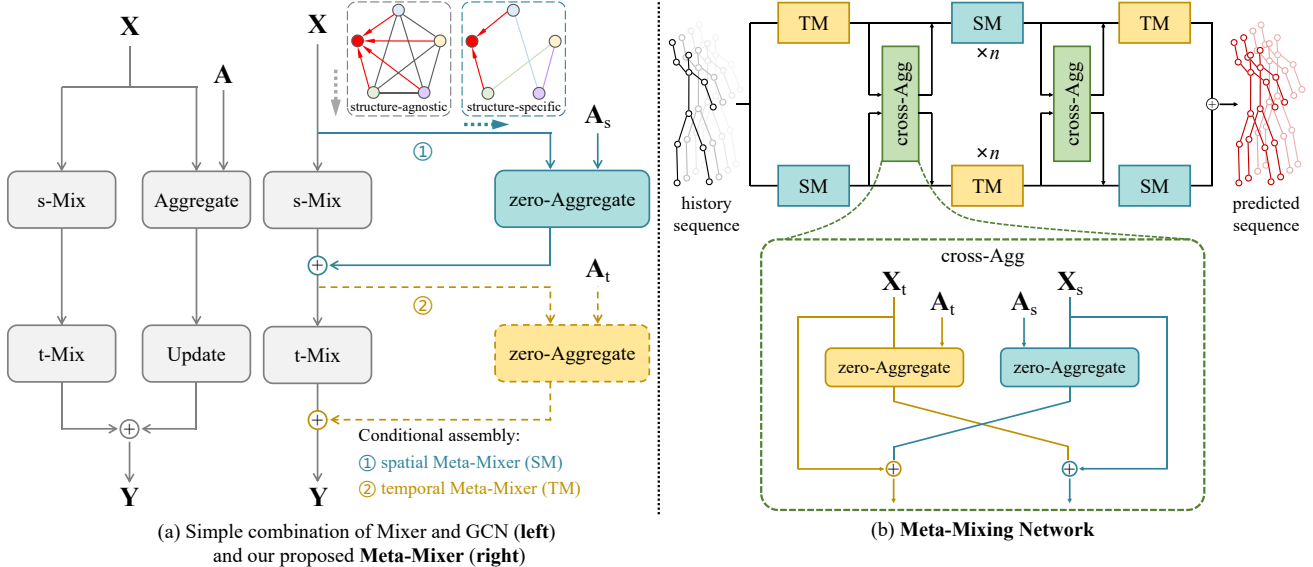


Figure 2. (Best viewed in color) **Our Meta-Mixing Network ( $M^2$ -Net)**. (a) Comparison between a simple combination of two models (left) and our proposed Meta-Mixer (right). (b) Our proposed network with Meta-Mixers as building blocks. “Zero-Aggregate” is a novel aggregation function where manually specified elements of the parameterized adjacency grow from zeros to optimized parameters in a learned manner. Different from a straightforward combination, our Meta-Mixer is developed from the theoretical analogy between Mixers and GCNs that a mixing layer can be seen as a particular case of a graph convolutional layer when it is applied to a fully-connected graph with parameterized adjacency. Combined with techniques such as parameter tying and the novel zero aggregation, the network captures both the structure-specific and structure-agnostic dependencies in a collaborative manner.

a proper architectural design, achieve competitive performance to CNNs and Transformers [36] besides being more computationally efficient. MLP-Mixer [33] is one of the works that mark the comeback of MLPs. In MLP-Mixer, each layer mainly involves two steps: token mixing and channel mixing, encoding the spatial information along the flattened spatial dimensions. [14] separately encodes the feature representations along the height and width dimensions with linear projections. Much like the re-entry of MLPs into computer vision, MLP-like models have also started to emerge in human motion prediction. In the spirit to explore non-graph convolutional alternatives, [1, 13] employ Mixer-like architectures which deliver state-of-the-art performance besides being more simple and efficient than GCNs. Their models are very much like MLP-Mixers, in which the patch and channel dimensions in MLP-Mixers are branded as spatial and temporal dimensions for motion sequence data. Current approaches in human motion prediction are either graph convolutional or mixer-like. We show in this paper that these two approaches can be unified.

### 3. Meta-Mixing Network

Suppose that a motion sequence consists of  $T$  consecutive frames, in which each pose has  $J$  joints. The motion sequence is denoted by  $S_{1:T} = [S_1, S_2, \dots, S_T] \in \mathbb{R}^{T \times J \times 3}$ . The task of human motion prediction is to predict the un-

known future sequence  $S_{T+1:T+T_f}$ , based on the observed history sequence  $S_{1:T}$ .

In Section 3.1, we present the unified perspective on Mixers and GCNs, which further gives rise to our method. We defer presenting the proposed method to Section 3.2.

#### 3.1. A Unified Perspective on GCNs and Mixers

We first briefly introduce Mixers and GCNs in the community. Then the bulk of this subsection presents how to unify GCNs and Mixers into a general approach.

Given a motion sequence of size  $T \times J \times 3$ , we first reshape it into a sequence of flattened poses. This results in a matrix  $\mathbf{X} = [x_1, x_2, \dots, x_N]^T \in \mathbb{R}^{N \times T}$ , with  $N = 3J$ . Each row vector  $x_n^T$  corresponds to the trajectory of a joint coordinate, and each column vector a flattened pose. In Mixer-based methods, the network employs MLPs to perform spatial mixing and temporal mixing along the two dimensions of  $\mathbf{X}$  respectively. In classic GCN-based methods,  $\mathbf{X}$  is treated as a graph with  $N$  nodes and  $T$  features for each node. Then the network performs graph convolutions over the graph based on trainable adjacencies.

Regardless of non-linearities such as activation function and normalization, which are simply legacy artifacts from old classic models, a mixer layer and a graph convolutional layer can both be implemented based on matrix multiplications. In each mixer layer, the channel-mixing transposes the input, right-multiplies it with a weight matrix  $\mathbf{W}_1$  and

then transposes back the product. The token-mixing then right-multiplies it with another weight matrix  $\mathbf{W}_2$ . These two mixing operations result in a combination of matrix products in the following form:

$$f_{\text{Mix}}(\mathbf{X}) = \mathbf{W}_1^\top \mathbf{X} \mathbf{W}_2, \quad (1)$$

where  $\mathbf{W}_1 \in \mathbb{R}^{N \times N}$  and  $\mathbf{W}_2 \in \mathbb{R}^{T \times T}$  are both trainable weight matrices implicitly given by the channel-mixing and token-mixing MLPs respectively. This function shows that the overall effect of a mixer layer can be seen as to left-multiply the input with a weight matrix then right-multiply it with another. Since the weight matrices are set as trainable parameters, the transpose of them does not make much of a difference on the practical side. The mixer layer bears a strong analogy to the graph convolutional layer in standard GCNs, which follows an aggregate-update paradigm. The aggregation can be implemented by left-multiplying the input with an adjacency matrix, and the update by right-multiplying it with a weight matrix. The overall action of a graph convolutional layer can be written as:

$$f_{\text{GraphConv}}(\mathbf{X}) = \mathbf{A} \mathbf{X} \mathbf{W}, \quad (2)$$

where  $\mathbf{A} \in \mathbb{R}^{N \times N}$  is the adjacency matrix and  $\mathbf{W} \in \mathbb{R}^{T \times T}$  is a trainable weight usually set as a square matrix.

Comparing Eq. 1 and Eq. 2, we make the following two findings. First, the update is the same as token-mixing. Second, the aggregation and channel-mixing both perform a linear combination of node or patch features (rows in  $\mathbf{X}$ ). Given element-wise notation as  $\mathbf{W}_1 = (w_{ij})$ , the  $i$ -th row of  $\mathbf{W}_1^\top \mathbf{X}$  is computed as:

$$[\mathbf{W}_1^\top \mathbf{X}]_{i,:} = \sum_{j=1}^N w_{ji} \mathbf{x}_j, \quad (3)$$

which means each patch feature after channel-mixing is a linear combination of all patch features. Likewise, given  $\mathbf{A} = (a_{ij})$  which specifies the relation from node  $j$  to node  $i$ , the  $i$ -th row of  $\mathbf{A}^\top \mathbf{X}$  is given by:

$$[\mathbf{A} \mathbf{X}]_{i,:} = \sum_{j=1}^N a_{ij} \mathbf{x}_j, \quad (4)$$

which means each aggregated feature of a node is a linear combination of features in its neighborhood.

Comparing Eq. 3 and Eq. 4, we see that the key factor differentiating a graph convolutional layer from a mixer layer is the use of adjacency information to linearly combine different features. The adjacency represents the structural relationships among data such as the skeleton joint-bone structure in the context of human motion prediction. If we remove such structural information from GCNs by,

for example, parameterizing the adjacency as trainable parameters, or if we feed adjacency information as an additional input to Mixers, graph convolutional layers and mixer layers can have the same effect on the input features. In other words, Mixers and GCNs are mainly distinguished by whether they are agnostic to the structural relationships between different patches or nodes. The main takeaway from this unified perspective is that a mixing layer can be seen as a particular case of a graph convolutional layer when it is applied to a fully-connected graph with parameterized adjacency. So far we have presented the unified perspective on GCNs and Mixers without considering non-linearities. It's worth noting that including the non-linearity is important to achieve strong performance for neural networks. To this end, we provide more in-depth discussions on unifying GCNs and Mixers without excluding the non-linearities in the supplementary material.

### 3.2. The Proposed Method

**Spatial and temporal mixing.** The mixing blocks adopt a similar design to those in [33, 13] which involve fully-connected layers, transpose operations and layer normalization. The spatial mixing (s-Mix) and temporal mixing (t-Mix) are defined using matrix operations as:

$$\begin{aligned} \mathbf{U} &= \mathcal{S}(\mathbf{X}; \Theta_1) = (\mathbf{X}^\top \mathbf{W}_{\theta_1})^\top; \\ \mathbf{Y} &= \mathcal{T}(\mathbf{U}; \Theta_2) = \mathbf{U} \mathbf{W}_{\theta_2}, \end{aligned} \quad (5)$$

where  $\mathcal{S}(\cdot; \Theta_1)$  is the spatial mixing function with a trainable weight matrix  $\mathbf{W}_{\theta_1} \in \mathbb{R}^{N \times N}$  parameterized by a set of parameters  $\Theta_1$ ,  $\mathcal{T}(\cdot; \Theta_2)$  is the temporal mixing function with a trainable weight matrix  $\mathbf{W}_{\theta_2} \in \mathbb{R}^{T \times T}$  parameterized by a set of parameters  $\Theta_2$ , and LN is layer normalization.

**Zero aggregation.** Mixers are known to deliver competitive performance on top of being computationally more efficient. We first want to preserve these advantages and then uplift them with prior structural knowledge we have about the data. To this end, we propose a novel zero aggregation. The zero aggregation operation is defined as:

$$\mathbf{Z} = \mathcal{Z}(\mathbf{A}, \mathbf{X}; \Theta) = (\mathbf{A} \circ \Theta) \mathbf{X}, \quad (6)$$

where  $\mathbf{A}$  is a pre-defined binary adjacency matrix as a universal input to each layer,  $\Theta$  is a trainable parameter matrix and  $\circ$  denotes the element-wise product.  $\mathbf{A}$  and  $\Theta$  are square matrices of the same shape, whose size is dependent on the assembly of Meta-Mixer.

**Meta-Mixer.** The Meta-Mixer is constructed with different flavors of assembly, resulting in a spatial Meta-Mixer (SM) or temporal Meta-Mixer (TM). The conditional assembly is based on the fact that matrix multiplications are

Mean Per Joint Position Error (in millimeter)								
milliseconds	80	160	320	400	560	720	880	1000
LTD-50-25 [28]	12.2	25.4	50.7	61.5	79.6	93.6	105.2	112.4
LTD-10-10 [28]	11.2	23.4	47.9	58.9	78.3	93.3	106.0	114.0
HisRep [27]	10.4	22.6	47.1	58.3	77.3	91.8	104.1	112.1
MSR-GCN [8]	11.3	24.3	50.8	61.9	80.0	-	-	112.9
PGBIG [25]	10.6	23.1	47.1	57.9	76.3	90.7	102.4	109.7
siMLPe [13]	9.6	21.7	46.3	57.3	75.7	90.1	101.8	109.4
Ours	<b>9.4</b>	<b>21.3</b>	<b>45.8</b>	<b>56.7</b>	<b>75.2</b>	<b>89.7</b>	<b>100.9</b>	<b>108.6</b>
STSGCN [30]†	10.1	17.1	33.1	38.3	50.8	60.1	68.9	75.6
GAGCN [39]†	10.1	16.9	32.5	38.5	50.0	-	-	72.9
MotionMixer [1]†	9.0	13.2	26.9	33.6	46.1	56.5	65.7	71.6
Ours†	<b>6.9</b>	<b>13.0</b>	<b>24.9</b>	<b>30.8</b>	<b>41.6</b>	<b>51.4</b>	<b>59.7</b>	<b>65.0</b>

Table 1. **Results on Human3.6M** at different prediction time steps in terms of mean per joint position error (MPJPE) in millimeter. 256 samples are tested for each action. † indicates methods that compute the average error over all frames, whose results are taken from the paper [1]. Otherwise, the methods are evaluated at each particular frame, whose results are taken from the paper [13]. We can see that our approach consistently outperforms other approaches under both evaluation protocols.

associative, so the order in which temporal and spatial mixing or aggregation and update are applied does not change the layer outcome. For the spatial Meta-Mixer block, its overall operation  $\mathcal{M}_s(\mathbf{X})$  is given by:

$$\begin{aligned} \mathbf{U} &= \text{LN}(\mathcal{S}(\mathbf{X}; \Theta_1) + \mathcal{Z}(\mathbf{A}_s, \mathbf{X}; \Theta_s)); \\ \mathbf{Y} &= \text{LN}(\mathcal{T}(\mathbf{U}; \Theta_2)), \end{aligned} \quad (7)$$

where  $\mathbf{A}_s \in \mathbb{R}^{N \times N}$  is a spatial adjacency matrix, which is specified by the skeleton’s joint-bone structure. the operation of temporal Meta-Mixer block  $\mathcal{M}_t(\mathbf{X})$  is given by:

$$\begin{aligned} \mathbf{U} &= \text{LN}(\mathcal{S}(\mathbf{X}; \Theta_1)); \\ \mathbf{Y} &= \text{LN}(\mathcal{T}(\mathbf{U}; \Theta_2) + \mathcal{Z}(\mathbf{A}_t, \mathbf{U}; \Theta_t)), \end{aligned} \quad (8)$$

where  $\mathbf{A}_t \in \mathbb{R}^{D \times D}$  is a temporal adjacency matrix, which is set as a tridiagonal matrix. The idea behind such a setting is to limit the neighborhood of each node across from its last frame to its next frame of the same joint.

To stabilize the training in the beginning stage, the parameters  $\Theta_s$  and  $\Theta_t$  in all of the zero aggregation operations are initialized as zeros and frozen for a few training steps. Therefore, in the first few training steps, we have:

$$\begin{cases} \mathcal{Z}(\mathbf{A}_s, \mathbf{X}; \Theta_s) = \mathbf{0}; \\ \mathcal{Z}(\mathbf{A}_t, \mathbf{U}; \Theta_t) = \mathbf{0}; \\ \mathcal{M}_s(\mathbf{X}) = \mathcal{M}_t(\mathbf{X}). \end{cases} \quad (9)$$

Comparing Eq. 9 with Eq. 7–8, we can see that, in the first few training steps, both the spatial Meta-Mixer blocks and the temporal Meta-Mixer blocks apply the same operations over the input features as basic mixer blocks do. In other words, in the first training stage, the network only employs fully-connected layers to capture structure-agnostic dependencies that are representative of those more common

and generic motion patterns. Once the parameters are unfrozen after the first training stage, they begin to progressively move from zeros to optimized directions. The Meta-Mixers are imbued with structural information of data to efficiently capture structure-specific dependencies in a fine tuning fashion under the guidance of adjacency. The motivation behind this is that an increase in parameters can lead to overfitting and slow learning. By this design, the network is sufficient to satisfy the theory, but is not so overparameterized so as to risk overfitting. We not only preserve the functionality and result quality of Mixers, but also uplift them with GCNs’ well-established capability to model structure-sensitive data based on adjacency.

**Architecture of Meta-Mixing Network.** The spatial and temporal Meta-Mixer blocks serve as the building blocks of the overall network, termed Meta-Mixing Network ( $M^2$ -Net). Figure 2 depicts the overall architecture of the proposed network. The network adopts a two-branch design assembled in a symmetrical fashion. In each branch, we employ a number  $n + 2$  of Meta-Mixing blocks in successive order. The first and the last blocks are differently assembled from the blocks in the middle. Aside from a series of Meta-Mixer blocks in each branch, we employ two fusion blocks between branches after the first blocks and before the last blocks respectively. The fusion blocks are implemented using zero aggregation to allow for the exchange of spatio-temporal features between branches in a fine tuning-like manner. The outputs of two branches are added together to produce the final output of the  $M^2$ -Net. Following [13], other components of the network include Discrete Cosine Transform (DCT), residual connection and data augmentation, which are consistent with theirs.

scenarios	Walking				Eating				Smoking				Discussion			
milliseconds	80	400	560	1000	80	400	560	1000	80	400	560	1000	80	400	560	1000
LTD-50-25 [28]	12.3	44.4	50.7	60.3	7.8	38.6	51.5	75.8	8.2	39.5	50.5	72.1	11.9	68.1	88.9	118.5
LTD-10-10 [28]	11.1	42.9	53.1	70.7	7.0	37.3	51.1	78.6	7.5	37.5	49.4	71.8	10.8	65.8	88.1	121.6
PGBIG [25]	11.2	42.8	49.6	58.9	6.5	36.8	50.0	74.9	7.3	37.5	48.8	69.9	10.2	64.4	86.1	116.9
siMLPe [13]	9.9	39.6	46.8	55.7	5.9	36.1	49.6	74.5	6.5	36.3	47.2	69.3	9.4	64.3	85.7	116.3
STSGCN [30]†	10.7	38.2	40.6	51.8	6.7	31.6	33.9	52.5	7.1	30.6	33.6	50.1	9.7	45.0	53.4	78.8
GAGCN [39]†	10.3	32.4	39.9	51.1	6.4	25.2	31.8	51.4	7.1	24.3	31.1	48.7	9.7	38.9	53.1	76.9
MotionMixer [1]†	7.3	28.6	-	49.2	4.3	20.9	-	47.4	4.7	21.4	-	45.4	6.4	35.5	-	78.0
Ours	9.3	38.6	45.9	55.6	5.6	34.1	48.6	74.3	6.3	36.3	46.8	68.8	9.2	63.4	84.3	115.0
Ours†	<b>6.9</b>	<b>24.6</b>	<b>30.5</b>	<b>40.1</b>	<b>4.3</b>	<b>18.9</b>	<b>26.0</b>	<b>42.6</b>	<b>4.5</b>	<b>19.7</b>	<b>26.5</b>	<b>41.2</b>	<b>6.1</b>	<b>33.2</b>	<b>45.9</b>	<b>71.9</b>
scenarios	Directions				Greeting				Phoning				Posing			
milliseconds	80	400	560	1000	80	400	560	1000	80	400	560	1000	80	400	560	1000
LTD-50-25 [28]	8.8	58.0	74.2	105.5	16.2	82.6	104.8	136.8	9.8	50.8	68.8	105.1	12.2	79.9	110.2	174.8
LTD-10-10 [28]	8.0	54.9	76.1	108.8	14.8	79.7	104.3	140.2	9.3	49.7	68.7	105.1	10.9	75.9	109.9	171.7
PGBIG [25]	7.5	56.0	73.3	105.9	14.0	77.3	100.2	136.4	8.7	48.8	66.5	102.7	10.2	73.3	102.8	167.0
siMLPe [13]	6.5	55.8	73.1	106.7	12.4	77.3	99.8	137.5	8.1	48.6	66.3	103.3	8.8	73.8	103.4	168.7
STSGCN [30]†	7.4	40.9	47.6	71.0	12.4	54.5	64.8	91.6	8.2	36.6	41.8	66.1	9.9	52.6	64.3	106.4
GAGCN [39]†	7.3	34.5	45.8	69.9	11.8	48.4	62.3	87.7	8.8	28.7	41.1	66.0	10.1	45.1	63.3	99.1
MotionMixer [1]†	4.4	29.2	-	66.5	8.8	46.2	-	93.6	5.6	27.8	-	63.4	6.0	40.1	-	99.7
Ours	5.9	55.7	72.1	106.8	12.4	76.2	99.4	134.5	7.7	47.8	66.0	103.1	8.8	72.5	100.7	165.3
Ours†	4.8	<b>28.0</b>	<b>39.0</b>	<b>62.2</b>	9.5	<b>40.9</b>	<b>54.8</b>	<b>84.1</b>	<b>5.5</b>	<b>25.8</b>	<b>35.5</b>	<b>58.4</b>	<b>5.8</b>	<b>36.0</b>	<b>51.7</b>	<b>90.7</b>
scenarios	Purchases				Sitting				Sitting Down				Taking Photo			
milliseconds	80	400	560	1000	80	400	560	1000	80	400	560	1000	80	400	560	1000
LTD-50-25 [28]	15.2	78.1	99.2	134.9	10.4	58.3	79.2	118.7	17.1	76.4	100.2	143.8	9.6	54.3	75.3	118.8
LTD-10-10 [28]	13.9	75.9	99.4	135.9	9.8	55.9	78.5	118.8	15.6	71.7	96.2	142.2	8.9	51.7	72.5	116.3
PGBIG [25]	13.2	74.0	95.7	132.1	9.1	54.6	75.1	114.8	14.7	70.0	94.4	139.0	8.2	50.2	70.5	112.9
siMLPe [13]	11.7	72.4	93.8	132.5	8.6	55.2	75.4	114.1	13.6	70.8	95.7	142.4	7.8	50.8	71.0	112.8
STSGCN [30]†	11.9	54.8	63.7	93.5	9.1	39.8	47.7	75.3	14.4	53.8	63.3	94.3	8.1	41.9	47.0	76.9
GAGCN [39]†	11.9	47.6	62.1	85.1	9.3	38.5	45.4	71.1	14.1	47.4	62.8	84.1	8.5	35.1	45.2	70.0
MotionMixer [1]†	8.4	42.7	-	88.7	6.5	29.8	-	68.9	10.9	42.6	-	89.3	5.5	27.9	-	66.6
Ours	10.5	70.7	92.4	129.1	8.1	53.8	74.8	113.8	13.7	69.2	95.6	138.6	7.8	49.8	72.1	114.3
Ours†	<b>8.6</b>	<b>38.5</b>	<b>51.5</b>	<b>78.8</b>	<b>6.5</b>	<b>28.7</b>	<b>39.8</b>	<b>65.5</b>	<b>10.7</b>	<b>39.5</b>	<b>52.8</b>	<b>83.0</b>	5.7	<b>26.5</b>	<b>37.1</b>	<b>62.5</b>
scenarios	Waiting				Walking Dog				Walking Together				Average			
milliseconds	80	400	560	1000	80	400	560	1000	80	400	560	1000	80	400	560	1000
LTD-50-25 [28]	10.4	59.2	77.2	108.3	22.8	88.7	107.8	156.4	10.3	46.3	56.0	65.7	12.2	61.5	79.6	112.4
LTD-10-10 [28]	9.2	54.4	73.4	107.5	20.9	86.6	109.7	150.1	9.6	44.0	55.7	69.8	11.2	58.9	78.3	114.0
PGBIG [25]	8.7	53.6	71.6	103.7	20.4	84.6	105.7	145.9	8.9	43.8	54.4	64.6	10.6	57.9	76.3	109.7
siMLPe [13]	7.8	53.2	71.6	104.6	18.2	83.6	105.6	141.2	8.4	41.2	50.8	61.5	9.6	57.3	75.7	109.4
STSGCN [30]†	8.6	40.7	47.3	72.0	17.6	66.4	74.7	102.6	8.6	35.1	38.9	51.1	10.1	38.3	51.7	75.6
GAGCN [39]†	8.5	33.8	45.9	69.3	17.0	59.4	70.1	91.3	-	-	-	-	10.1	38.5	50.0	72.9
MotionMixer [1]†	5.4	30.0	-	68.2	13.4	54.1	-	99.6	5.9	27.4	-	50.4	9.0	33.6	-	71.6
Ours	7.6	51.8	73.0	102.7	19.0	84.2	105.1	140.4	8.5	40.9	52.4	63.6	9.4	56.7	75.2	108.6
Ours†	5.7	<b>27.6</b>	<b>38.3</b>	<b>61.6</b>	<b>13.3</b>	<b>49.7</b>	<b>63.5</b>	<b>90.5</b>	<b>5.8</b>	<b>23.8</b>	<b>30.6</b>	<b>42.5</b>	<b>6.9</b>	<b>30.8</b>	<b>41.6</b>	<b>65.0</b>

Table 2. **Action-wise results on Human3.6M** at different prediction time steps in terms of MPJPE in millimeter. 256 samples are tested for each action. † indicates methods that compute the average error over all frames, whose results are taken from the paper [1]. Otherwise, the methods are evaluated at each particular frame, whose results are taken from the paper [13]. Our model achieves state-of-the-art performance on nearly all actions and time steps, especially as the prediction time grows.

## 4. Experiment

### 4.1. Datasets

**Human3.6M (H3.6M).** H3.6M [15] is a large-scale dataset for human-related tasks. It involves 15 types of actions performed by 7 actors. Following the normality of previous work, We preprocess the data to remove global rotation and translation, discard redundant joints, and downsample the sequence to 25fps. Then we convert the data to 3D coordinates for the final training, validation and test sets. Each

pose is characterized by 22 joints with their corresponding 3D coordinates. We use subject 11 and subject 5 for validation and testing respectively, and the remaining 5 subjects for training, following previous work.

**AMASS.** AMASS [26] is a collection of multiple Mo-cap datasets unified by SMPL parameterization. Following [13], we use AMASS-BMLrub as the test set and split the rest of the AMASS dataset into training and validation sets.

**3D Pose in the Wild (3DPW).** The 3DPW dataset [37] covers activities captured from both indoor and outdoor

scenes. Following [13] we evaluate 18 joints using the model trained on AMASS to evaluate generalization.

## 4.2. Experimental Setup

**Evaluation Metrics.** We report the experimental results in terms of the Mean Per Joint Position Error (MPJPE), which is the most preferred metric in the community. The lower the MPJPE, the better the performance.

**Implementation Details.** We implemented our network using Pytorch. We trained the model on NVIDIA RTX 3080 Ti GPU for 60k iterations with a batch size of 256. We used Adam optimizer [16] with learning rate starting at 0.0005 and dropping to 0.000005 after 55k iterations.

## 4.3. Comparison with State-of-the-Art Methods

In this subsection we report quantitative results of state-of-the-art methods and ours for motion prediction on H3.6M, AMASS and 3DPW. We also present qualitative evaluation by visualizing predicted samples.

**Comparison on Human3.6M.** The H3.6M dataset is the currently most preferred dataset for evaluating the performance of human motion prediction methods. We first present the quantitative results on H3.6M with the utmost detail and precision. We also provide qualitative results of different methods by visualizing some predicted samples in H3.6M. Following [13], we test 256 samples for each action. The baseline methods follow two different testing protocols, one as in [27] where the errors are computed at each time step, and the other as in [30] where the errors are computed by averaging all time steps. In fair comparison, we evaluate our method under both of the two testing protocols. The two protocols are differentiated by a † sign. In Table 1, we compare our methods with other state-of-the-art methods in terms of average MPJPEs for all actions on average at different time steps. Our method achieves the best results under both testing protocols. For more comparison, we also report the action-wise results of all 15 actions in Table 2.

**Comparison on AMASS and 3DPW.** We report the results on AMASS and 3DPW in Table 3. Following [13], the models are trained on AMASS and tested on AMASS-BMLrub and 3DPW. There are two different evaluation protocols following [30] and [28] respectively. We evaluate our method under both two evaluation protocols.

## 4.4. Ablation Study

In this subsection, we conduct a series of ablation experiments on the essential components of our network to analyze the advantages of our method.

**Importance of Meta-Mixing.** We first show that unifying GCNs and Mixers into Meta-Mixer is important and necessary for the task, which is the theoretical motivation of our proposed Meta-Mixing Network. We demonstrate this

argument in a progressive way. First, we build a baseline model which is a simple combination of GCN and Mixer with a two-stream design, whose outputs are added at the end of each layer. Then we gradually incorporate each essential component into this simple model, with the following assembly choices: **a)** share parameters between the update and temporal mixing; **b)** replace the aggregation with our proposed zero aggregation in parallel with spatial mixing; **c)** share parameters between the aggregation and spatial mixing; **d)** replace the update with our proposed zero aggregation in parallel with temporal mixing; **e)** construct two parallel branches with symmetric assembly to one another; **f)** adding fusion blocks across two branches. The results in Table 4 verify the importance and necessity of unifying Mixers and GCNs into a general approach rather than simply combining them. It also shows the advantages brought by techniques used in our network such as parameter tying and the proposed zero aggregation.

**Ablation on network architecture.** Next we ablate on different design choices for the network. First, we assemble the network such that each branch has the same type of Meta-Mixer blocks, instead of interleaved spatial and temporal blocks in each branch. Second, we apply fusion connections after each block. Third, we use the same type of blocks to assemble the entire network. The results under each of these settings are shown in Table 5, which verifies the effectiveness of our network architecture.

**Role of the model scale.** We show the influence of model scaling on our network by decreasing or increasing the number of Meta-Mixer blocks in Table 6. We see that our model achieves its best with 48 blocks.

## 4.5. Visualization

To put a finer point on the evaluation of our method, we present various qualitative results. Figure 3 provides samples of walking pose sequences predicted by ours and [13] on H3.6M, which shows that our method generates more realistic and accurate poses. To thoroughly analyze the superiority of our network, we show the effect of zero aggregation in Figure 4 (a). The pose represented by solid lines is the final output of the network, while the pose of dashed lines is obtained during inference with zero aggregation blocks manually set to zeros, thereby eliminating their influence. These dashed lines demonstrate the structure-agnostic dependencies learned by basic mixers, which are not sufficient for accurate motion prediction. The differences between the two poses, highlighted by the red lines, stress the importance of learning structure-specific dependencies based on adjacency information, as can also be developed from the visualization of the learned network components in Figure 4 (b). Overall, these results underscore

Dataset	AMASS-BMLrub								3DPW							
	80	160	320	400	560	720	880	1000	80	160	320	400	560	720	880	1000
convSeq2Seq [19]	20.6	36.9	59.7	67.6	79.0	87.0	91.5	93.5	18.8	32.9	52.0	58.8	69.4	77.0	83.6	87.8
LTD-10-10 [28]	10.3	19.3	36.6	44.6	61.5	75.9	86.2	91.2	12.0	22.0	38.9	46.2	59.1	69.1	76.5	81.1
LTD-10-25 [28]	11.0	20.7	37.8	45.3	57.2	65.7	71.3	75.2	12.6	23.2	39.7	46.6	57.9	65.8	71.5	75.5
HisRep [27]	11.3	20.7	35.7	42.0	51.7	58.6	63.4	67.2	12.6	23.1	39.0	45.4	56.0	63.6	69.7	73.7
siMLPe [13]	10.8	19.6	34.3	40.5	50.5	57.3	62.4	65.7	12.1	22.1	38.1	44.5	54.9	62.4	68.2	72.2
Ours	<b>10.4</b>	<b>19.1</b>	38.9	<b>40.2</b>	<b>50.1</b>	<b>56.6</b>	<b>61.9</b>	<b>65.4</b>	<b>12.0</b>	<b>22.1</b>	<b>37.8</b>	<b>44.1</b>	<b>54.5</b>	<b>62.1</b>	<b>68.0</b>	72.3

Table 3. Results on AMASS and 3DPW at different prediction time steps. The results are taken from the paper [13].

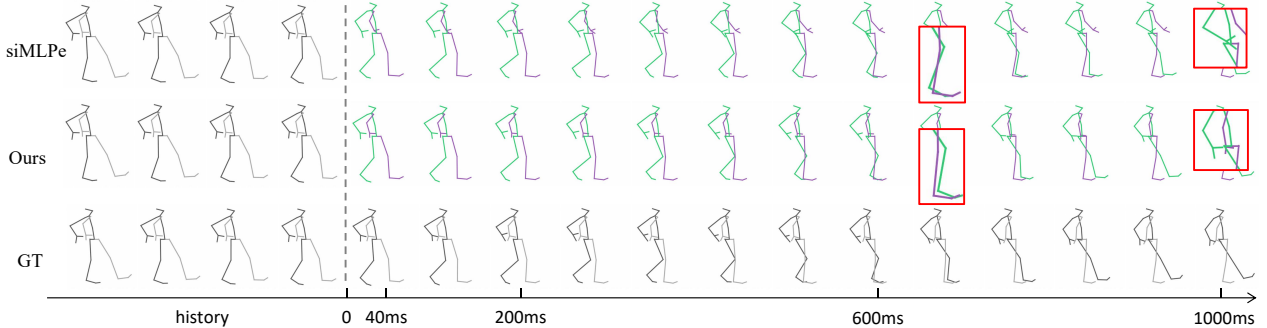


Figure 3. Qualitative results on H3.6M. We visualize a walking sample of predicted pose sequences and their ground truths.

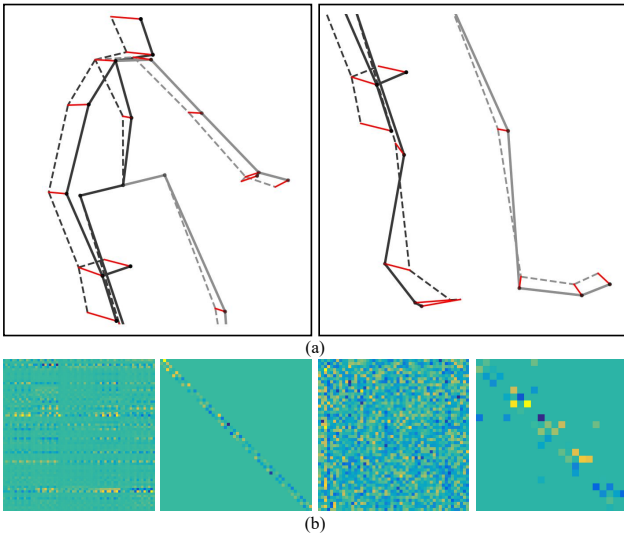


Figure 4. Visualization results. (a) Effect of zero aggregation. Solid lines depict the pose learned by the overall network; dashed lines depict the pose learned from structure-agnostic dependencies without zero aggregation, the differences between which are highlighted by red lines, which represent the structure-specific dependencies. (c) Visualization of the learned spatial Meta-Mixer, spatial adjacency and their temporal counterparts (from left to right).

the superiority of our approach.

#### 4.6. Conclusion

In this paper, we first provide a unified perspective on MLP-Mixers and GCNs. We show that they bear a strong analogy in terms of how the individual layer looks, and

Setting	80	160	320	400	560	1000
baseline	10.1	22.5	47.4	58.5	78.3	115.0
a	10.2	23.0	48.1	59.1	78.0	113.2
a,b	10.2	22.6	47.7	59.0	77.7	112.2
c	11.2	25.1	51.5	62.6	81.2	114.4
c,d	10.1	22.7	47.6	58.9	77.5	112.5
a,b,c,d	9.7	21.7	45.9	56.8	75.4	109.3
a,b,c,d,e	9.6	21.7	45.8	56.8	75.3	109.0
a,b,c,d,e,f (default)	<b>9.4</b>	<b>21.3</b>	<b>45.8</b>	<b>56.7</b>	<b>75.2</b>	<b>108.6</b>

Table 4. Ablation on Meta-Mixer. Each group of settings labeled a–f (see “Importance of Meta-Mixing”) results in a different model that is used to evaluate the critical components of Meta-Mixer.

Design choice	80	160	320	400	560	1000
w/o interleave	9.7	22.1	46.8	57.9	76.8	110.3
full fuse	10.4	23.0	47.6	58.6	77.6	112.4
all SM	9.7	21.8	46.2	57.1	75.8	109.7
all TM	10.2	22.6	47.2	58.3	77.0	111.0
Default	<b>9.4</b>	<b>21.3</b>	<b>45.8</b>	<b>56.7</b>	<b>75.2</b>	<b>108.6</b>

Table 5. Ablation on network architecture. “w/o interleave” means each branch has the same type of blocks instead of interleaved ones. “full fuse” means applying fusion connections after each block. “all SM” and “all TM” means using the same type of blocks to assemble the entire network.

thus can be generalized into an approach that exploits advantages from both sides. In human motion prediction, we find that both the structure-agnostic and structure-specific information is necessary, because human motion is intrinsically ruled by skeletal structure and shares similarity in motion patterns. However, current approaches largely do not include this information into their networks. Based

Nb. Blocks	Param. (M)	FLOPs	80	560	1000
12	0.26	1.4G	10.1	77.5	113.2
24	0.50	2.5G	9.9	76.4	111.7
48 (default)	0.96	4.9G	<b>9.4</b>	<b>75.2</b>	<b>108.6</b>
64	1.30	6.5G	9.5	75.2	109.9
96	1.95	9.6G	9.7	75.4	110.2

Table 6. **Ablation on the number of blocks.** The best result is achieved with 48 blocks with less than one million parameters.

on our theoretical findings, we propose Meta-Mixing Network. With a novel zero aggregation operation, our network is capable of capturing both the structure-agnostic and the structure-sensitive dependencies in a collaborative manner.

## References

- [1] Arij Bouazizi, Adrian Holzbock, Ulrich Kressel, Klaus Dietmayer, and Vasileios Belagiannis. Motionmixer: mlp-based 3d human body pose forecasting. *arXiv preprint arXiv:2207.00499*, 2022. [1](#), [3](#), [5](#), [6](#), [15](#)
- [2] Joan Bruna, Wojciech Zaremba, Arthur Szlam, and Yann LeCun. Spectral networks and locally connected networks on graphs. *arXiv preprint arXiv:1312.6203*, 2013. [2](#)
- [3] Judith Butepage, Michael J Black, Danica Kragic, and Hedvig Kjellstrom. Deep representation learning for human motion prediction and classification. In *IEEE/CVF Conference on Computer Vision and Pattern Recognition (CVPR)*, pages 6158–6166, 2017. [2](#)
- [4] Shoufa Chen, Enze Xie, Chongjian Ge, Ding Liang, and Ping Luo. Cyclemlp: A mlp-like architecture for dense prediction. *arXiv preprint arXiv:2107.10224*, 2021. [1](#)
- [5] Jaesung Choe, Chung Hyun Park, Francois Rameau, Jaesik Park, and In So Kweon. Pointmixer: Mlp-mixer for point cloud understanding. In *Computer Vision—ECCV 2022: 17th European Conference, Tel Aviv, Israel, October 23–27, 2022, Proceedings, Part XXVII*, pages 620–640. Springer, 2022. [1](#)
- [6] François Chollet. Xception: Deep learning with depthwise separable convolutions. In *Proceedings of the IEEE conference on computer vision and pattern recognition*, pages 1251–1258, 2017. [2](#)
- [7] Qiongjie Cui, Huaijiang Sun, and Fei Yang. Learning dynamic relationships for 3d human motion prediction. In *IEEE/CVF Conference on Computer Vision and Pattern Recognition (CVPR)*, pages 6519–6527, 2020. [2](#)
- [8] Lingwei Dang, Yongwei Nie, Chengjiang Long, Qing Zhang, and Guiqing Li. Msr-gcn: Multi-scale residual graph convolution networks for human motion prediction. In *IEEE/CVF International Conference on Computer Vision (ICCV)*, pages 11467–11476, 2021. [2](#), [5](#), [11](#)
- [9] Katerina Fragkiadaki, Sergey Levine, Panna Felsen, and Jitendra Malik. Recurrent network models for human dynamics. In *IEEE/CVF International Conference on Computer Vision (ICCV)*, pages 4346–4354, 2015. [2](#)
- [10] Partha Ghosh, Jie Song, Emre Aksan, and Otmar Hilliges. Learning human motion models for long-term predictions. In *International Conference on 3D Vision (3DV)*, pages 458–466, 2017. [2](#)
- [11] Anand Gopalakrishnan, Ankur Mali, Dan Kifer, Lee Giles, and Alexander G Ororbia. A neural temporal model for human motion prediction. In *IEEE/CVF Conference on Computer Vision and Pattern Recognition (CVPR)*, pages 12116–12125, 2019. [2](#)
- [12] Jianyuan Guo, Yehui Tang, Kai Han, Xinghao Chen, Han Wu, Chao Xu, Chang Xu, and Yunhe Wang. Hire-mlp: Vision mlp via hierarchical rearrangement. In *Proceedings of the IEEE/CVF Conference on Computer Vision and Pattern Recognition*, pages 826–836, 2022. [2](#)
- [13] Wen Guo, Yuming Du, Xi Shen, Vincent Lepetit, Xavier Alameda-Pineda, and Francisc Moreno-Noguer. Back to mlp: A simple baseline for human motion prediction. In *Proceedings of the IEEE/CVF Winter Conference on Applications of Computer Vision*, pages 4809–4819, 2023. [1](#), [3](#), [4](#), [5](#), [6](#), [7](#), [8](#), [12](#), [13](#), [15](#)
- [14] Qibin Hou, Zihang Jiang, Li Yuan, Ming-Ming Cheng, Shuicheng Yan, and Jiashi Feng. Vision permutator: A permutable mlp-like architecture for visual recognition. *IEEE Transactions on Pattern Analysis and Machine Intelligence*, 45(1):1328–1334, 2022. [1](#), [2](#), [3](#)
- [15] Catalin Ionescu, Dragos Papava, Vlad Olaru, and Cristian Sminchisescu. Human3.6m: Large scale datasets and predictive methods for 3d human sensing in natural environments. *IEEE Transactions on Pattern Analysis and Machine Intelligence (PAMI)*, 36(7):1325–1339, 2013. [6](#)
- [16] Diederik P Kingma and Jimmy Ba. Adam: A method for stochastic optimization. *ArXiv:1412.6980*, 2014. [7](#)
- [17] Thomas N Kipf and Max Welling. Semi-supervised classification with graph convolutional networks. *ArXiv:1609.02907*, 2016. [1](#), [2](#), [13](#)
- [18] Colin Lea, Michael D Flynn, Rene Vidal, Austin Reiter, and Gregory D Hager. Temporal convolutional networks for action segmentation and detection. In *proceedings of the IEEE Conference on Computer Vision and Pattern Recognition*, pages 156–165, 2017. [2](#)
- [19] Chen Li, Zhen Zhang, Wee Sun Lee, and Gim Hee Lee. Convolutional sequence to sequence model for human dynamics. In *IEEE/CVF Conference on Computer Vision and Pattern Recognition (CVPR)*, pages 5226–5234, 2018. [2](#), [8](#)
- [20] Maosen Li, Siheng Chen, Zihui Liu, Zijing Zhang, Lingxi Xie, Qi Tian, and Ya Zhang. Skeleton graph scattering networks for 3d skeleton-based human motion prediction. In *Proceedings of the IEEE/CVF international conference on computer vision*, pages 854–864, 2021. [2](#)
- [21] Maosen Li, Siheng Chen, Zijing Zhang, Lingxi Xie, Qi Tian, and Ya Zhang. Skeleton-parted graph scattering networks for 3d human motion prediction. In *Computer Vision—ECCV 2022: 17th European Conference, Tel Aviv, Israel, October 23–27, 2022, Proceedings, Part VI*, pages 18–36. Springer, 2022. [2](#)
- [22] Maosen Li, Siheng Chen, Yangheng Zhao, Ya Zhang, Yanfeng Wang, and Qi Tian. Dynamic multiscale graph neural networks for 3d skeleton based human motion prediction. In *IEEE/CVF Conference on Computer Vision and Pattern Recognition (CVPR)*, pages 214–223, 2020. [1](#), [2](#), [11](#)
- [23] Maosen Li, Siheng Chen, Yangheng Zhao, Ya Zhang, Yanfeng Wang, and Qi Tian. Multiscale spatio-temporal graph

- neural networks for 3d skeleton-based motion prediction. *IEEE Transactions on Image Processing (TIP)*, 30:7760–7775, 2021. [2](#)
- [24] Dongze Lian, Zehao Yu, Xing Sun, and Shenghua Gao. As-mlp: An axial shifted mlp architecture for vision. *arXiv preprint arXiv:2107.08391*, 2021. [1](#)
- [25] Tiezheng Ma, Yongwei Nie, Chengjiang Long, Qing Zhang, and Guiqing Li. Progressively generating better initial guesses towards next stages for high-quality human motion prediction. In *IEEE/CVF Conference on Computer Vision and Pattern Recognition (CVPR)*, pages 6437–6446, 2022. [1](#), [2](#), [5](#), [6](#), [15](#)
- [26] Naureen Mahmood, Nima Ghorbani, Nikolaus F Troje, Gerard Pons-Moll, and Michael J Black. Amass: Archive of motion capture as surface shapes. In *Proceedings of the IEEE/CVF international conference on computer vision*, pages 5442–5451, 2019. [6](#)
- [27] Wei Mao, Miaomiao Liu, and Mathieu Salzmann. History repeats itself: Human motion prediction via motion attention. In *Computer Vision—ECCV 2020: 16th European Conference, Glasgow, UK, August 23–28, 2020, Proceedings, Part XIV 16*, pages 474–489. Springer, 2020. [5](#), [7](#), [8](#), [11](#)
- [28] Wei Mao, Miaomiao Liu, Mathieu Salzmann, and Hongdong Li. Learning trajectory dependencies for human motion prediction. In *IEEE/CVF International Conference on Computer Vision (ICCV)*, pages 9489–9497, 2019. [1](#), [2](#), [5](#), [6](#), [7](#), [8](#), [11](#), [15](#)
- [29] Wei Mao, Miaomiao Liu, Mathieu Salzmann, and Hongdong Li. Multi-level motion attention for human motion prediction. *International journal of computer vision*, 129(9):2513–2535, 2021. [1](#)
- [30] Theodoros Sofianos, Alessio Sampieri, Luca Franco, and Fabio Galasso. Space-time-separable graph convolutional network for pose forecasting. In *IEEE/CVF International Conference on Computer Vision (ICCV)*, pages 11209–11218, 2021. [1](#), [2](#), [5](#), [6](#), [7](#), [11](#)
- [31] Chuanxin Tang, Yucheng Zhao, Guangting Wang, Chong Luo, Wenxuan Xie, and Wenjun Zeng. Sparse mlp for image recognition: Is self-attention really necessary? In *Proceedings of the AAAI Conference on Artificial Intelligence*, volume 36, pages 2344–2351, 2022. [2](#)
- [32] Yehui Tang, Kai Han, Jianyuan Guo, Chang Xu, Yanxi Li, Chao Xu, and Yunhe Wang. An image patch is a wave: Phase-aware vision mlp. In *Proceedings of the IEEE/CVF Conference on Computer Vision and Pattern Recognition*, pages 10935–10944, 2022. [1](#)
- [33] Ilya O Tolstikhin, Neil Houlsby, Alexander Kolesnikov, Lucas Beyer, Xiaohua Zhai, Thomas Unterthiner, Jessica Yung, Andreas Steiner, Daniel Keysers, Jakob Uszkoreit, et al. Mlp-mixer: An all-mlp architecture for vision. *Advances in neural information processing systems*, 34:24261–24272, 2021. [1](#), [2](#), [3](#), [4](#), [13](#), [15](#)
- [34] Hugo Touvron, Piotr Bojanowski, Mathilde Caron, Matthieu Cord, Alaeldin El-Nouby, Edouard Grave, Gautier Izacard, Armand Joulin, Gabriel Synnaeve, Jakob Verbeek, et al. Resmlp: Feedforward networks for image classification with data-efficient training. *IEEE Transactions on Pattern Analysis and Machine Intelligence*, 2022. [1](#), [2](#)
- [35] Zhengzhong Tu, Hossein Talebi, Han Zhang, Feng Yang, Peyman Milanfar, Alan Bovik, and Yinxiao Li. Maxim: Multi-axis mlp for image processing. In *Proceedings of the IEEE/CVF Conference on Computer Vision and Pattern Recognition*, pages 5769–5780, 2022. [2](#)
- [36] Ashish Vaswani, Noam Shazeer, Niki Parmar, Jakob Uszkoreit, Llion Jones, Aidan N Gomez, Łukasz Kaiser, and Illia Polosukhin. Attention is all you need. *Advances in neural information processing systems*, 30, 2017. [3](#)
- [37] Timo Von Marcard, Roberto Henschel, Michael J Black, Bodo Rosenhahn, and Gerard Pons-Moll. Recovering accurate 3d human pose in the wild using imus and a moving camera. In *Proceedings of the European conference on computer vision (ECCV)*, pages 601–617, 2018. [6](#)
- [38] Tan Yu, Xu Li, Yunfeng Cai, Mingming Sun, and Ping Li. S2-mlp: Spatial-shift mlp architecture for vision. In *Proceedings of the IEEE/CVF Winter Conference on Applications of Computer Vision*, pages 297–306, 2022. [1](#), [2](#)
- [39] Chongyang Zhong, Lei Hu, Zihao Zhang, Yongjing Ye, and Shihong Xia. Spatio-temporal gating-adjacency gcn for human motion prediction. In *Proceedings of the IEEE/CVF Conference on Computer Vision and Pattern Recognition*, pages 6447–6456, 2022. [5](#), [6](#)
- [40] Honghong Zhou, Caili Guo, Hao Zhang, and Yanjun Wang. Learning multiscale correlations for human motion prediction. In *IEEE International Conference on Development and Learning (ICDL)*, pages 1–7, 2021. [2](#)

# — Supplementary Material —

## A. Overview

The supplementary material includes sections as follows:

- Section **B**: Efficiency analysis and comparison.
- Section **C**: Qualitative comparison with other methods and analysis of zero aggregation through visualization.
- Section **D**: A more inclusive perspective on unifying MLP-Mixers and GCNs with each of their essential components taken into consideration.
- Section **E**: Meta-Mixer as a generalization of popular Mixer and GCN models in the community.

## B. Analysis of Computational Efficiency

In the main text, we give an in-depth presentation of our proposed Meta-Mixer, which has superior theoretical capacity compared to MLP-Mixers and GCNs and achieves state-of-the-art performance. Ensuring efficiency is also a key challenge for deep networks besides improving theoretical capacity. Here we provide an extensive analysis of computational efficiency in terms of layer-wise and overall complexity, parameter size and computational cost.

**Computational complexity.** Given an input matrix  $\mathbf{X} \in \mathbb{R}^{N \times T}$  of  $N$  patches or nodes with  $T$  features, current GCNs in the community [28, 8, 30], like many convolutional networks, project node representations into some high-dimensional latent space to aggregate messages and update representations. For example, LTD [28] encodes node features into 256-dimensional hidden presentations to which graph convolutions are applied. Let  $\mathbf{H} \in \mathbb{R}^{N \times T_h}$  denote the hidden representations. A graph convolutional layer is defined as  $\mathbf{Y} = \sigma(\mathbf{A}\mathbf{H}\mathbf{W})$  where  $\mathbf{A} \in \mathbb{R}^{N \times N}$  is the adjacency matrix,  $\mathbf{W} \in \mathbb{R}^{T_h \times T_h}$  is the weight matrix and  $\sigma$  denotes an element-wise non-linearity. The computational complexity of each graph convolutional layer is:

$$O_{GC}(N^2T_h + NT_h^2 + NT_h). \quad (\text{A. 1})$$

Since  $T_h$  is usually much bigger than  $T$ , it results in a considerable amount of parameters and computational cost.

In contrast, MLP-Mixers are well known for their superior efficiency by doing away with convolutions, which require additional computational costs due to matrix multiplication with specialized implementation. The MLP-Mixer can be simplified to bring down computational costs

Model	Standard GCN [28]	M <sup>2</sup> -Net (ours)
Complex. per layer	$O(N^2T_h + NT_h^2 + NT_h)$	$O(N^2T + NT^2 + 2N^2)$
Complex. all layers	$O(130.1M)$	$O(\mathbf{23.2M})$ (↓ 82.3%)
Param.	2.56M	<b>0.96M</b> (↓ 62.5%)
FLOPs	21.6G	<b>4.9G</b> (↓ 77.3%)

Table 7. **Comparison of efficiency** between standard GCNs and our M<sup>2</sup>-Net in terms of layer-wise complexity, all-layer complexity, parameter size and computational cost. In common settings, we have  $N = 66$ ,  $T = 35$  and  $T_h = 256$ . The proposed M<sup>2</sup>-Net is considerably more efficient than GCNs.

even more. For example, our Meta-Mixer employs single-layered MLPs instead of double-layered MLPs (see Section **D**), which means excluding the GELU and preserving the input size. A layer of spatial Meta-Mixer can be expressed as  $\mathbf{Y} = (\mathbf{W}_1 + (\mathbf{A}_s \circ \Theta_s))\mathbf{X}\mathbf{W}_2$ , where  $\mathbf{A}_s$ ,  $\Theta_s$  and  $\mathbf{W}_1$  are of the same size  $N \times N$ , and  $\mathbf{W}_2$  is of size  $T \times T$ , which results in a computational complexity of:

$$O_{SM}(N^2T + NT^2 + 2N^2). \quad (\text{A. 2})$$

A layer of temporal Meta-Mixer can be expressed as  $\mathbf{Y} = \mathbf{W}_1\mathbf{X}(\mathbf{W}_2 + (\mathbf{A}_t \circ \Theta_t))$ , where  $\mathbf{A}_t$ ,  $\Theta_t$  and  $\mathbf{W}_2$  are of the same size  $T \times T$ , and  $\mathbf{W}_1$  is of size  $N \times N$ , resulting in:

$$O_{TM}(N^2T + NT^2 + 2T^2). \quad (\text{A. 3})$$

As can be seen from the analysis above, the computational cost of our Meta-Mixer is much lower than that of GCNs, given that  $T_h$  is much larger than  $T$ . For example, in the long-term setting for Human3.6M, we have  $N = 66$  and  $T = 35$ . If we choose  $T_h = 256$  which is commonly adopted in [28, 22, 27, 8], the computational complexity of a graph convolution layer adds up to  $O_{GC}(5457408)$ , and our spatial and temporal Meta-Mixer layers have the complexity of  $O_{SM}(242022)$  and  $O_{TM}(235760)$ . The computational complexity of our Meta-Mixer layers is only 4% of that of GCN layers. Besides layer-wise comparison, the overall all-layer complexity is reported in Table 7, which shows that our M<sup>2</sup>-Net has %82.3 less all-layer complexity than LTD.

**Parameter size and computational cost.** In order to apply graph convolutions to high-dimensional hidden representations, GCNs require more parameters and memory consumption. For example, updating 256-dimensional node

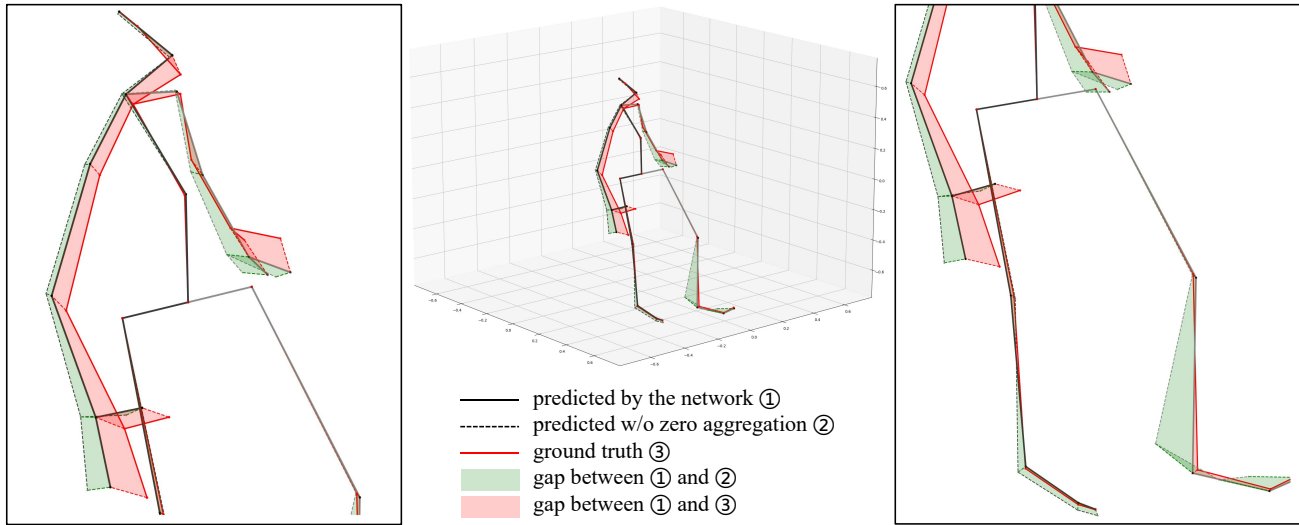


Figure 5. **Effect of zero aggregation** in a representative walking action case. Lines of different colors and styles correspond to poses at 1000ms predicted by the model with or without zero aggregation blocks and the corresponding ground truth. Their differences from one another are highlighted by shaded areas between them. The area in green represents the contribution of zero aggregation to the final prediction, which reflects the structure-specific dependencies captured by zero aggregation. Comparing the areas in green and red, we see that the zero aggregation blocks are able to adaptively adjust the poses based on different joint positions characterized by diverse motion patterns, driving the prediction closer to ground truths.

features requires a weight matrix involving  $2^{16}$  trainable parameters. Apart from the computational cost brought by operating on higher-dimensional hidden representations, current GCNs largely employ activation functions and batch normalization following each layer, which further decreases their efficiency. To thoroughly analyze the efficiency of the overall networks, we also report the comparison between GCNs and our  $M^2$ -Net in terms of parameter size and FLOPs. As shown in Table 7, our  $M^2$ -Net is considerably more efficient than typical GCNs.

### C. Visualizations

In this section, we provide more experimental results by visualization to analyze the strengths of our method.

**Importance of zero aggregation.** In order to thoroughly demonstrate the importance of the zero aggregation blocks in our  $M^2$ -Net, we visualize the effect of zero aggregation for all actions in Figure 5. Each sub-figure shows the last pose in the predicted pose sequence for each action. Consistent with the main text, solid lines represent poses predicted by the model. Dashed lines represent poses predicted by the model with all zero aggregation blocks fixed at zeros during inference, which is thus agnostic to the skeleton structural information. The Red lines connecting the joints of solid poses and dashed poses highlight the contribution of zero aggregation blocks to the final prediction, which reflects the structure-specific dependencies. As can be seen across different action cases, the zero aggregation blocks are able to

adaptively adjust the poses based on different joint positions characterized by diverse motion patterns.

**Predicted pose sequences.** In the main text we illustrate visualized samples of actions that are more common and regular such as walking. Next we present more qualitative results for more sophisticated actions on H3.6M to showcase the superiority of  $M^2$ -Net compared to the latest state-of-the-art model, siMLPe [13]. Figure 6 provides several complex action cases including “posing”, “purchases” and “taking photo” from top to bottom. Actions such as walking exhibit simple and more or less periodic patterns involving arms and legs all moving in a regular and repetitive style, and are therefore relatively easier to predict. In contrast, complex actions are characterized by partial body movements without so much of a periodic pattern, for example, with several body parts moving and the other parts remaining still. As can be seen in the figure, in these complex action cases, the poses predicted by our model are closer to ground truths than those predicted by siMLPe. Another observation is that in cases of history pose sequences without easily visible movement, their model tends to produce poses that are little different from one another, whereas our model perceives those subtle changes and reflects the true motion patterns in the prediction.

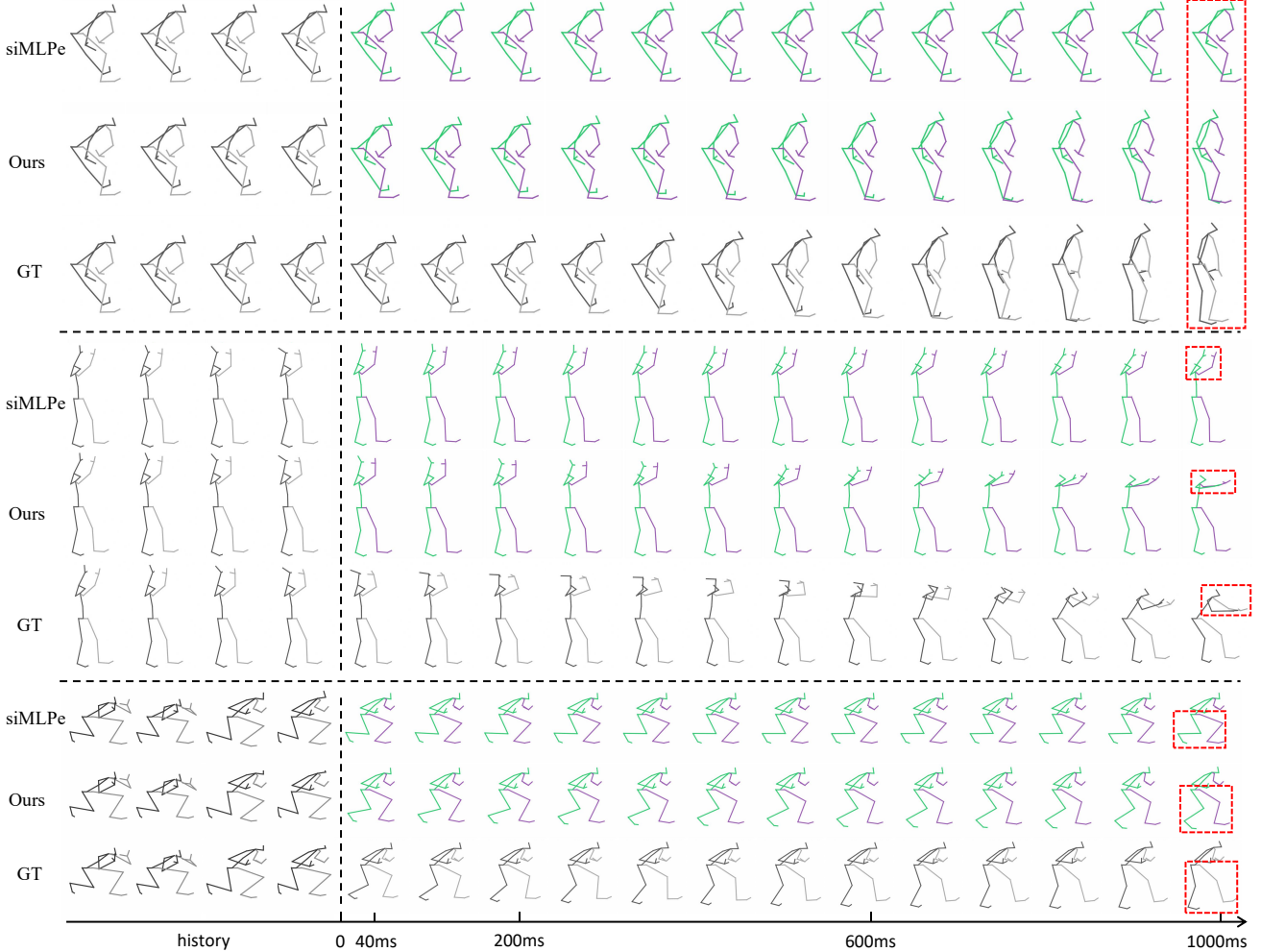


Figure 6. More qualitative comparison of  $M^2$ -Net with the latest state-of-the-art method, siMLPe [13]. From top to bottom are visualized samples of predicted poses and corresponding ground truths for “posing”, “purchases” and “taking photo”.

#### D. A More Inclusive Perspective on Unifying MLP-Mixers and GCNs

In the main text, we unify MLP-Mixers [33] and GCNs [17] in a simplified way that excludes certain components of their models such as non-linearity and using two fully-connected layers in each mixing MLP. However, the inclusion of these components is known to be important for their models to achieve great performance. To this end, we here present the unified perspective in more detail without excluding these components.

**Double-layered MLP.** In the original design of MLP-Mixer, each token-mixing or channel-mixing MLP consists of two fully-connected layers, which can be implemented using two weight matrices instead of one. The token-MLP and channel-MLP are defined as:

$$\begin{aligned} \mathbf{U} &= \text{token-MLP}(\mathbf{X}) = (\mathbf{X}^\top \mathbf{W}_1 \mathbf{W}_2)^\top; \\ \mathbf{Y} &= \text{channel-MLP}(\mathbf{U}) = \mathbf{U} \mathbf{W}_3 \mathbf{W}_4, \end{aligned} \quad (\text{A. 4})$$

where  $\mathbf{X} = [\mathbf{x}_1, \mathbf{x}_2, \dots, \mathbf{x}_N]^\top \in \mathbb{R}^{N \times T}$  is the input of  $N$  patches or nodes with  $T$  features,  $\mathbf{W}_1 \in \mathbb{R}^{N \times N'}$ ,  $\mathbf{W}_2 \in \mathbb{R}^{N' \times N}$ ,  $\mathbf{W}_3 \in \mathbb{R}^{D \times D'}$  and  $\mathbf{W}_4 \in \mathbb{R}^{D' \times D}$  are trainable parameters.  $N'$  and  $D'$  are selected independently of the input size. If given element-wise notation  $\mathbf{W}_1 = (\tilde{w}_{ij})$  and  $\mathbf{W}_2 = (\hat{w}_{mn})$ , we have:

$$\mathbf{U}_{n,:} = \sum_{m=1}^{N'} \sum_{i=1}^N \hat{w}_{mn} \tilde{w}_{im} \mathbf{x}_i^\top, \quad (\text{A. 5})$$

meaning that each patch feature after channel-mixing is a linear combination of all patch features, as in the case of single-layered MLPs described in the main text.

From a graph convolution point of view, let a graph be  $G = (\mathcal{V}, \mathcal{E})$ , where  $\mathcal{V} = \{1, 2, \dots, N\}$  is set of  $N$  nodes,  $\mathcal{E} \subseteq \mathcal{V} \times \mathcal{V}$  is a set of edges defined as order pairs  $(j, i)$  pointing from node  $j$  to  $i$ . A graph convolutional layer follows an aggregate-update (message passing) paradigm,

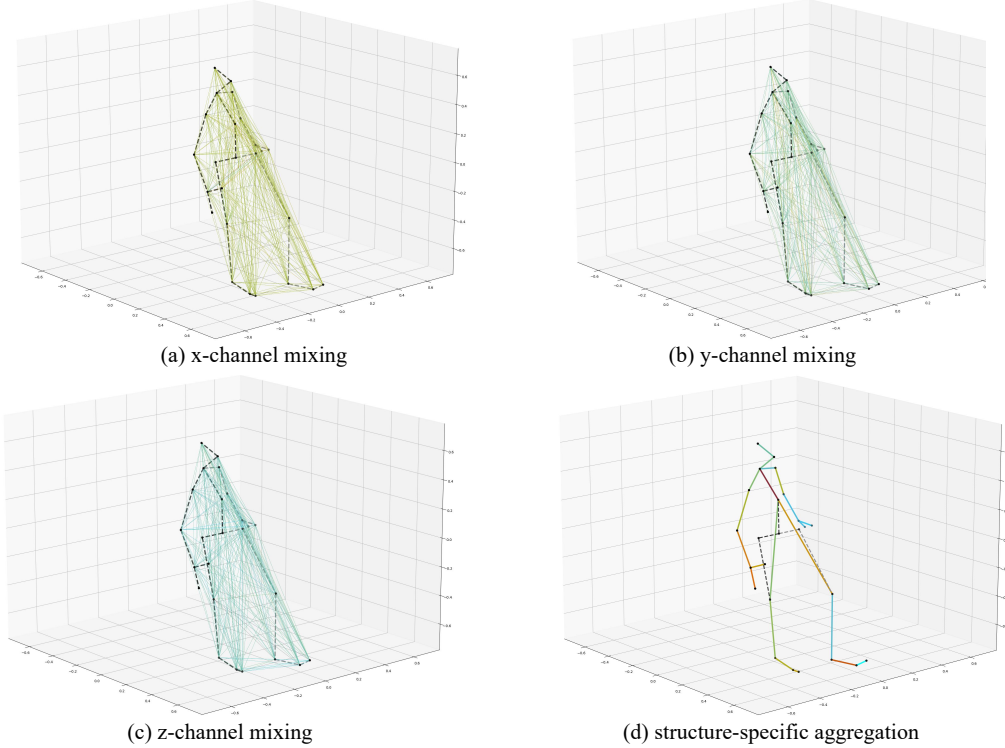


Figure 7. **Visualization of mixing and aggregation weights.** (a), (b) and (c) illustrate the linear combination weights among all nodes for the structure-agnostic mixing. (d) illustrates the aggregation weights between adjacent joint pairs for the structure-specific aggregation.

where each node aggregates some message from its neighborhood and combines the message with its features from the last iteration to obtain the new updated features. The mixer layer can be seen as a graph convolution layer applied to a fully-connected graph with weighted edges. Specifically, let  $e_{k\ell}$  denote the weight of the edge pointing from node  $k$  to node  $\ell$ . If the update matrix is given by  $\mathbf{W}_3\mathbf{W}_4$  and the edge weight  $e_{k\ell}$  satisfies the following equation:

$$e_{k\ell} = \sum_{j=1}^{N'} \hat{w}_{jk} \tilde{w}_{\ell j}, \quad (\text{A. 6})$$

then the graph convolutional layer is specialized to the mixer layer defined in Eq. A. 4. This mixer layer can be rewritten in the style of message passing in the following form:

$$\begin{aligned} \mathbf{m}_n &= \text{aggregate}(\{\mathbf{x}_k | k \in \mathcal{V} \setminus \{n\}\}) \\ &= \sum_{k=1, k \neq n}^N e_{kn} \mathbf{x}_k; \\ \mathbf{y}_n &= \text{update}(\mathbf{m}_n, \mathbf{x}_n) = \mathbf{W}_4^\top \mathbf{W}_3^\top (\mathbf{m}_n + \mathbf{x}_n), \end{aligned} \quad (\text{A. 7})$$

where  $\mathbf{W}_3$  and  $\mathbf{W}_4$  are the same as in Eq. A. 4 and  $e_{kn}$  is given by Eq. A. 6. Ultimately,  $\mathbf{y}_n^\top$  equals the  $n$ -th row vector of  $\mathbf{Y}$  in Eq. A. 4, which means that the mixer layer and the

graph convolutional layer have the same overall effect over the input patch/node features. Therefore, the mixer layer can be seen as a specialized graph convolutional layer.

**Non-linearity.** The non-linearity is also an essential component of both Mixers and GCNs. The MLP-Mixer employs a GELU between two fully-connected layers in each MLP. The inclusion of non-linearity into Eq. A. 4 results in:

$$\begin{aligned} \mathbf{U} &= \text{token-MLP}(\mathbf{X}) = (\sigma(\mathbf{X}^\top \mathbf{W}_1) \mathbf{W}_2)^\top; \\ \mathbf{Y} &= \text{channel-MLP}(\mathbf{U}) = \sigma(\mathbf{U} \mathbf{W}_3) \mathbf{W}_4, \end{aligned} \quad (\text{A. 8})$$

where  $\sigma$  denotes an element-wise non-linearity such as GELU or Tanh. Because the non-linearity is applied element-wise, the mixer layer can still be rewritten in the form of node-level message passing in the graph convolutional layer as:

$$\begin{aligned} \mathbf{m}_n &= \text{aggregate}(\{\mathbf{x}_k | k \in \mathcal{V}\}) \\ &= \sum_{m=1}^{N'} \hat{w}_{mn} \sigma\left(\sum_{k=1}^N \tilde{w}_{km} \mathbf{x}_k\right); \\ \mathbf{y}_n &= \text{update}(\mathbf{m}_n, \mathbf{x}_n) = \mathbf{W}_4^\top \sigma(\mathbf{W}_3^\top \mathbf{m}_n), \end{aligned} \quad (\text{A. 9})$$

where  $\mathbf{y}_n^\top$  equals the  $n$ -th row vector of  $\mathbf{Y}$  in Eq. A. 8, which corresponds to the features of the  $n$ -th node or patch. The two equations above show that, compared to linear

cases, the token-mixing or update step applies non-linear transformations, and that in channel-mixing or aggregation, the mixed or aggregated features are a non-linear combination of all patch or node features. Therefore, with the inclusion of non-linearity, the unified perspective on Mixers and GCNs still holds.

## E. Meta-Mixer as Generalization of Popular Mixer and GCN Models

In the main text, we propose Meta-Mixer, which is derived from the unified perspective on Mixers and GCNs. In this section, we show how existing state-of-the-art Mixer and GCN-based models in human motion prediction generalize to our Meta-Mixer.

LTD [28] is one of the classic GCN models in the community, which relies on graph convolution with fully-trainable adjacency without extra constraints. This exclusion of skeleton adjacency information makes their model nothing short of what an MLP-Mixer is able to achieve. The difference between their model and a standard MLP-Mixer is merely the choice of non-linearity such as activation function and normalization. Therefore, LTD model can generalize to our Meta-Mixer.

PGBIG [25] applies spatial-temporal graph convolution to input features. Each of their graph convolutional layers has two fully-trainable adjacency matrices defined in spatial and temporal domains respectively. The spatial graph convolution can be seen as a particular case of our spatial Meta-Mixer when the zero aggregation blocks are fixed with zeros. Likewise, the temporal graph convolution can be seen as a special temporal Meta-Mixer. Overall, their graph convolutional layer can be seen as a spatial Meta-Mixer block and a temporal Meta-Mixer block integrated into one block, which can be easily achieved by fixing certain parameters and removing certain non-linearity components.

siMLPe [13] and MotionMixer [1] borrow the idea of Mixer into human motion prediction. Their mixer models are very much like the original MLP-Mixer [33]. A few adaptations include dispensing with GELU non-linearity, applying channel and patch dimensions to temporal and spatial dimensions, and changing the network architecture. In terms of the mixer layer, both of them can be seen as our Meta-Mixer with zero aggregation blocks fixed at zeros, which deprives their models of the capability of exploiting skeleton structural information.